Experimental Observation of Vacancy-assisted Martensitic Transformation Shift in Ni-Fe-Ga Alloys

I. Unzueta,[1,2,*] D. Alonso de R-Lorente,[3] E. Cesari,[4] V. Sánchez-Alarcos,[3,5] V. Recarte,[3,5] J. I. Pérez-Landazábal,[3,5] J. A. García,[6,2] and F. Plazaola[1]

[1]*Department of Electricity and Electronics, University of the Basque Country UPV/EHU, 48940 Leioa, Spain*
[2]*BCMaterials, University of Basque Country UPV/EHU, 48940 Leioa, Spain*
[3]*Department of Science, Universidad Pública de Navarra, Campus de Arrosadía, 31006 Pamplona, Spain*
[4]*Department of Physics, Universitat de les Illes Balears, Ctra. de Valldemossa, km 7.5, E-07122, Palma de Mallorca, Spain*
[5]*Institute for Advanced Materials (INAMAT), Universidad Pública de Navarra, Campus de Arrosadía, 31006 Pamplona, Spain*
[6]*Department of Applied Physics II, University of the Basque Country UPV/EHU, 48940 Leioa, Spain*

(Received 9 October 2018; published 23 April 2019)

Positron annihilation lifetime spectroscopy is used to experimentally demonstrate the direct relationship between vacancies and the shift of the martensitic transformation temperature in a $Ni_{55}Fe_{17}Ga_{28}$ alloy. The evolution of vacancies assisting the ordering enables shifts of the martensitic transformation up to 50 K. Our results confirm the role that both vacancy concentration and different vacancy dynamics play in samples quenched from the $L2_1$ and $B2$ phases, which dictate the martensitic transformation temperature and its subsequent evolution. Finally, by electron-positron density functional calculations V_{Ni} is identified as the most probable vacancy present in $Ni_{55}Fe_{17}Ga_{28}$. This work evidences the capability of vacancies for the fine-tuning of the martensitic transformation temperature, paving the way for defect engineering of multifunctional properties.

DOI: 10.1103/PhysRevLett.122.165701

The plethora of multifunctional properties that Ni-based Ni_2YZ Heusler alloys display, such as giant magnetoresistance [1,2], the magnetocaloric effect [3,4], large magnetic-field-induced strain [5,6], and shape-memory effect [7] are linked to the occurrence of the so-called martensitic transformation (MT). MT is a first order diffusionless phase transformation based on electronic properties [8,9] and driven by Jahn-Teller splitting [10]. These promising features, however, are hindered by the poor mechanical properties that these alloys present [11]. In this context, Ni-Fe-Ga systems are increasingly attracting great interest due to their mechanical properties and their consequent enhanced deformation behavior [12–14]. The improved ductility performance in bulky off-stoichiometric samples makes the Ni-Fe-Ga system a promising alternative to the classic Ni-Mn-Ga alloys [15]. Recently, a giant reversible elastocaloric effect has been reported in Ni-Fe-Ga alloys near room temperature [16].

Hereby, the control of the MT and its related features acquire a key relevance for a proper optimization of the aforementioned functional properties. For instance, in Ni-Mn based Heusler alloys and in Ni-Fe-Ga systems, the composition [17] and doping [18,19] are the main factors affecting the MT temperature (T_{MT}). In the Ni-Fe-Ga system, the composition can be tuned to get a T_{MT} near room temperature [20]. Additionally, the microstructure plays a key role on the MT characteristics [21]. The magnetism of Ni-Fe-Ga atoms is mainly confined to the Fe sites and the variation of Fe-Fe distances affects strongly the exchange coupling [22,23]. Moreover, the degree of long-range atomic order is found to affect strongly both T_c Curie's temperature and T_{MT}, which in some Ni-Mn based alloys enables shifts of T_{MT} (ΔT_{MT}) of about 100 K [24].

Several works have considered the potential role of vacancies on MT. Ren and Otsuka [25,26] demonstrate that the short-range atomic order during MT requires the diffusion of point defects to stabilize the MT. As vacancies assist the diffusion and the ordering process, they could also affect the MT. Indeed, Zhang *et al.* [27] speculate that vacancies could be the source of the observed entropy change in some Heusler Alloy ribbons. Other works point out the influence that vacancies may have on the pinning of MT [28–30]. In connection with the ordering process, Sánchez-Alarcos *et al.* and Santamarta *et al.* suggest different vacancy dynamics as responsible for the changes observed in T_c [31] and T_{MT} [32–34] in Ni-Mn-Ga and Ni-Fe-Ga alloys, respectively. Hsu *et al.* [35] indicate that vacancies may drive the $L2_1 \rightarrow B2$ order-disorder transition. However, none of the above suggestions have been experimentally proven, being the elusive nature of vacancies which has made it less experimentally investigated compared to other physical factors. As far as we know, there is no experimental proof of vacancies assisting the aforementioned processes in the literature.

The vast majority of works have been conducted within a theoretical framework, where formation energies of

different types of vacancy defects are calculated [36–40]. Recent works, by first principles calculations [41] and Monte Carlo simulations [42] link vacancies with the ordering process and their potential effect on T_{MT}. Regarding the experimental reports, the most complete study so far has been conducted by Merida *et al.* [43,44] in a Ni-Mn-Ga system by positron annihilation lifetime spectroscopy (PALS). However, no evidence linking the vacancy concentration (C_v) and ΔT_{MT} has been reported. In the present work, by combining PALS and differential scanning calorimetry (DSC), it is experimentally demonstrated that there is a direct relationship between vacancies and ΔT_{MT} in $Ni_{55}Fe_{17}Ga_{28}$ alloy. It is also proven that the different evolution of T_{MT} exhibited by samples quenched from $L2_1$ or $B2$ phases is linked to different vacancy dynamics in each case. Besides, PALS measurements and density functional theory (DFT) calculations point out that Ni vacancies are the most probable defects involved with ΔT_{MT}.

The synthesized $Ni_{55}Fe_{17}Ga_{28}$ polycrystalline samples (see Supplemental Material [45]) were quenched to ice water from temperatures ranging from 673 up to 1173 K in 100 K steps. Samples are labeled according to their quenching temperature (T_q) as Q673K, Q773K, and so forth. The influence of T_q on T_{MT} has been evaluated by DSC measurements. As shown in Fig. 1(a), for samples quenched from $T_q < 900$ K, T_{MT} increases along with T_q increase. However, for samples with $T_q > 900$ K, T_{MT} decreases as T_q increases. In Ni-Mn based Heusler alloys and in Ni-Fe-Ga alloys, T_{MT} is highly sensitive to the atomic order [33,65–67]. Indeed, as opposed to other Ni-Mn alloys [68], a less ordered $L2_1$ phase results in a higher T_{MT} [33,69]. Thus, the observed increment of T_{MT} for the samples quenched from $T_q < 900$ K indicates that for higher T_q, the retained $L2_1$ order degree is lower. However, for samples quenched from $T_q > 900$ K, T_{MT} decreases with the increasing T_q, denoting a higher degree of $L2_1$ order retained during quenching.

The different dependencies of T_{MT} on T_q shown by the as-quenched (AQ) samples matches the occurrence of a second neighbor ordering transition at 930 K (T_{L2_1-B2}), see Fig. 1(a). Thereby, it implies that while Q673, Q773, and Q873 samples have been quenched within the same structure (from $L2_1$ to $L2_1$), samples Q973, Q1073, and Q1173 have been quenched from the $B2$ phase to $L2_1$. Santamarta *et al.* [33,70] and Oikawa *et al.* [34] ascribe the dependency that the evolution of T_{MT} has on T_q, to different C_v for the $L2_1$ and $B2$ phases, which would promote different long-range atomic order retained during quenching. Moreover, previous works on Fe-Ni systems also show the dependence of T_{MT} on T_q, which has been also ascribed to the presence of quenched-in vacancies [35]. However, none of the previous works contribute any experimental evidence supporting their claims.

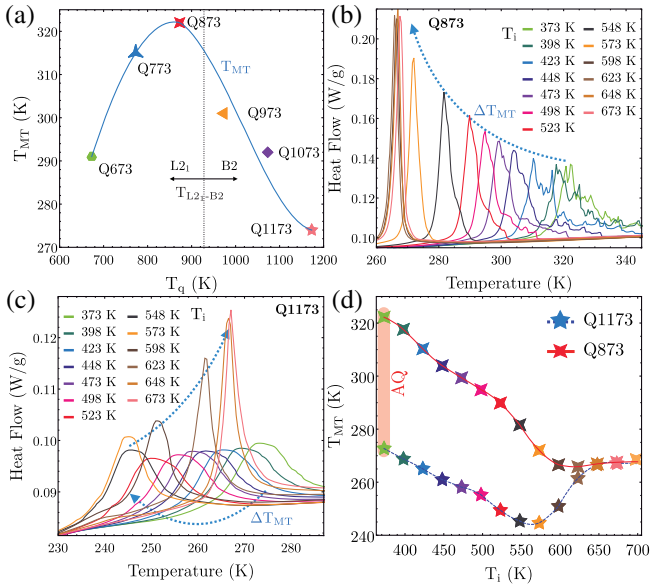

FIG. 1. (a) Direct T_{MT} versus T_q for all quenched samples. (b) Direct DSC curves for the 873 and (c) 1173 samples for each IAC. (d) The evolution of T_{MT} of Q873 and Q1173 samples as a function of the isochronal annealing temperature T_i.

As vacancies mediate the ordering process via diffusion [43], a different C_v could explain the observed phenomena. In this context, the powerful combination of PALS and DFT theory have been proven to be one of the most accurate techniques for the advanced characterization of vacancy defects in metals and semiconductors [71,72]. Thus, in order to ascertain the potential role of vacancies on the ΔT_{MT}, PALS experiments, along with theoretical positron lifetime calculations have been conducted on $Ni_{55}Fe_{17}Ga_{28}$ samples.

Figure 2(a) shows the experimental average positron lifetime values ($\bar{\tau}$) for samples Q1173 and Q873. As discussed in the Supplemental Material [45], spectra could not be decomposed because $\bar{\tau}$ is in a saturation trapping regime [73]. Anyway, for a given defect (one positron trap), $\bar{\tau}$ only depends on C_v, and the relation between $\bar{\tau}$ and C_v is given by the so-called one-trap model [45],

$$C_v = \frac{1}{\tau_b \mu_v} \frac{\bar{\tau} - \tau_b}{\tau_v - \bar{\tau}}, \tag{1}$$

where $\mu_v = 1.5 \times 10^{14}\ s^{-1}$ [43,44,74,75] is the specific trapping rate, $\tau_b = 106$ ps the theoretically calculated bulk lifetime (see Table I), and $\tau_v = 178$ ps [see Fig. 2(a)]. As inferred from Eq. (1) and evidenced in Fig. 2(b), a larger $\bar{\tau}$ implies a larger C_v.

The inset of Fig. 2(a) shows $\bar{\tau}$ values of AQ Q1173 (AQ1173) and AQ Q873 (AQ873) samples measured in both the austenite ($Fm\bar{3}m$, yellow region) and martensite ($I4/mmm$, blue region) phases. As indicated by the area shaded in red, the $\bar{\tau}$ value of sample AQ1173 measured in

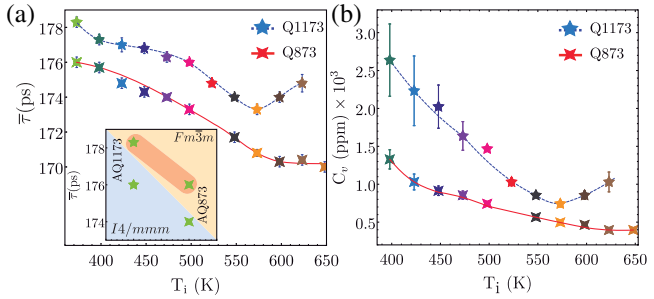

FIG. 2. PALS measurements of the samples quenched above (Q1173), and below (Q873) T_{L2_1-B2}. (a) The measured $\bar{\tau}$ and (b) the corresponding C_v calculated by means of Eq. (1) with $\tau_b = 106$ and $\tau_v = 178$ ps. The inset in (a) show the $\bar{\tau}$ values of AQ1173 and AQ873 samples measured in both the austenite ($Fm\bar{3}m$, yellow region) and martensite ($I4/mmm$, blue region) phases.

the $Fm\bar{3}m$ phase is higher than the one of AQ873. The same trend is observed for samples AQ1173 and AQ873 measured in the $I4/mmm$ phase, indicating that the B2 phase is characterized by larger C_v than the $L2_1$ phase. A larger C_v results in a larger supply of vacancies, which assist more effectively the ordering process during quenching. The larger C_v gives rise to an enhanced $L2_1$ order degree in sample AQ1173, which explains the lower T_{MT} that AQ1173 exhibits compared to AQ873 sample [see Fig. 1(a) and the area shaded in red of Fig. 1(d)].

In order to study the vacancy dynamics in samples quenched above and below the T_{L2_1-B2}, AQ samples were subjected to isochronal annealing cycles (IAC). IAC consist of heating up the samples up to a maximum temperature (T_i) (from 398 to 698 K every 25 K) at a constant rate of 10 K/ min. Then, after reaching T_i samples are cooled down at the same rate to the initial temperature. Figure 2 shows the evolution of both $\bar{\tau}$ and C_v (which inherits the same evolution of $\bar{\tau}$), as a function of T_i for Q873 and Q1173 samples. The most outstanding fact is the different behavior of $\bar{\tau}$ (and C_v) for Q1173 and Q873 in respect to T_i. For sample Q873, C_v decreases monotonically with T_i increase, while for sample Q1173 C_v decreases until $T_i \approx 570$ K. Then, from that temperature on, C_v increases as T_i does, indicating different vacancy dynamics for samples quenched above and below T_{L2_1-B2}.

TABLE I. Structural parameters used in theoretical calculations. The last column gathers the theoretical defect-related positron lifetime values calculated by $\gamma(\mathbf{r})^{\mathrm{BN}}_{\mathrm{LDA}}$ parameterization.

Phase Ref. [76]	Atom	Cell parameters Site	Occupancy	τ_v $\gamma(\mathbf{r})^{\mathrm{BN}}_{\mathrm{LDA}}$
	V_{Ni}	$8c$ (1/4, 1/4, 1/4)	1.00	178 ps
Austenite	$V^{\mathrm{Fe}}_{\mathrm{Ni}}$	$4a$ (0, 0, 0)	0.16	180 ps
$Fm\bar{3}m$, 225	V_{Ga}	$4b$ (1/2, 1/2, 1/2)	1.00	181 ps
$a = 5.774$ Å	$V^{\mathrm{Fe}}_{\mathrm{Ga}}$	$4a$ (0, 0, 0)	0.08	180 ps
	V_{Fe}	$4a$ (0, 0, 0)	0.76	181 ps
	Bulk	$(\cdots)$	$(\cdots)$	106 ps
	V_{Ni}	$4d$ (0, 1/2, 1/4)	1.00	176 ps
Martensite	$V^{\mathrm{Fe}}_{\mathrm{Ni}}$	$2a$ (0, 0, 0)	0.16	178 ps
$I4/mmm$, 139	V_{Ga}	$2b$ (0, 0, 1/2)	1.00	178 ps
$a=b=5.818$ Å	$V^{\mathrm{Fe}}_{\mathrm{Ga}}$	$2a$ (0, 0, 0)	0.08	178 ps
$c = 6.49600$ Å	V_{Fe}	$2a$ (0, 0, 0)	0.76	178 ps
	Bulk	$(\cdots)$	$(\cdots)$	104 ps

For the sake of comparison, the evolution of T_{MT} is also tracked by means of IAC. Figures 1(b) and 1(c) show a detailed shape of the DSC thermogram peaks for samples Q873K and Q1173K, respectively. In sample Q873K T_{MT} decreases monotonically with increasing T_i. However, T_{MT} for sample Q1173 initially decreases with T_i increase, but above $T_i \approx 570$ K, T_{MT} increases along with T_i. In fact, the same behavior is reproduced for all the samples with $T_q < T_{L2_1-B2}$ and $T_q > T_{L2_1-B2}$ (see Ref. [45]). In a nutshell, as shown in Fig. 1(d), the shift of T_{MT} also shows a different behavior depending on whether the sample is quenched above or below the T_{L2_1-B2} temperature. Additionally, the evolution of C_v with respect to T_i matches with the evolution of T_{MT} with respect to T_i, which suggests that different vacancy dynamics may play a role in the dependency that the shift of T_{MT} shows on T_q (see Figs. 1 and 2).

In order to complement the experimental PALS results, DFT calculations of the positron lifetime in $Ni_{55}Fe_{17}Ga_{28}$ alloy were performed using the atomic superposition method [77], which provides satisfactory values for metals and semiconductors [78–80]. Positron lifetime calculations were performed for exact $Ni_{55}Fe_{17}Ga_{28}$ composition, where the excess Ni and Ga atoms have been placed in Fe positions [76,81]. By overlapping the $n_+(\mathbf{r})$ positron density with the $n_-(\mathbf{r})$ electron density of the $Ni_{55}Fe_{17}Ga_{28}$, the annihilation rate $\lambda = \tau^{-1}$ was evaluated by

$$\lambda = \tau^{-1} = \pi c r_0^2 \int n_+(\mathbf{r}) n_-(\mathbf{r}) \gamma(\mathbf{r}) d\mathbf{r}, \qquad (2)$$

where c is the speed of light in vacuum, r_0 the classical electron radius, and $\gamma(\mathbf{r})$ the so-called enhancement factor that comprises the enhanced electron density due to the positron Coulombic attraction. $n_-(\mathbf{r})$ has been constructed by adding individual atomic charge densities around $\mathbf{R}_i$ atomic positions for the perfect lattice (bulk) and defected lattice, with different types of possible vacancies. In off-stoichiometric conditions, the excess Ni and Ga occupy the Fe sites [76,81], thus leading to two nonequivalent positions of both Ni and Ga, and a single Fe position [see Figs. 3(a) and 3(b)]. As a consequence, five types of vacancy defects are possible: V_{Ni}, V_{Fe}, and V_{Ga}, and vacancies of antisite atoms $V^{\mathrm{Fe}}_{\mathrm{Ni}}$ and $V^{\mathrm{Fe}}_{\mathrm{Ga}}$. The last vacancies refer to vacancies of antisite Ga and Ni excess atoms occupying natural Fe positions [76,81]. Calculations were

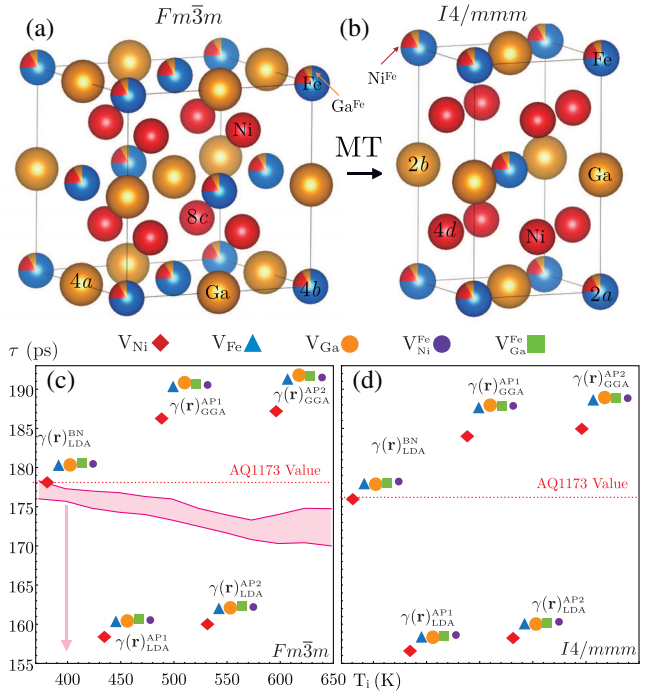

FIG. 3. Illustration of the (a) austenite and (b) martensite phases of Ni-Fe-Ga alloy. The calculated defect-related characteristic lifetimes for several possible types of vacancies, as well as for five different parametrizations of $\gamma(\mathbf{r})$ (c) for the $Fm\bar{3}m$ phase, and (d), for the $I4/mmm$ phase. The red-dashed lines indicate experimental AQ $\bar{\tau}$ values. The red shaded area illustrates the experimentally measured $\bar{\tau}$ range in the austenite phase.

carried out in unrelaxed $Fm\bar{3}m$ and $I4/mmm$ structures. Table I gathers the crystallographic data of the structures used in the calculations [45].

The enhancement factor $\gamma(\mathbf{r})$ of Eq. (2) has been modeled within the local density (LDA) and generalized gradient (GGA) approximations using five different parametrizations, labeled $\gamma(\mathbf{r})^{\mathrm{BN}}_{\mathrm{LDA}}$, $\gamma(\mathbf{r})^{\mathrm{AP1}}_{\mathrm{LDA}}$, $\gamma(\mathbf{r})^{\mathrm{AP2}}_{\mathrm{LDA}}$, $\gamma(\mathbf{r})^{\mathrm{AP1}}_{\mathrm{GGA}}$, and $\gamma(\mathbf{r})^{\mathrm{AP2}}_{\mathrm{GGA}}$ (for exact expressions see the Supplemental Material [45]). Results of the calculated defect-related positron lifetimes are illustrated in Figs. 3(c) and 3(d), respectively. The area shaded in red indicates the range of experimental $\bar{\tau}$ values. Calculated bulk lifetimes are not explicitly shown since in all cases τ_b ranges between 100 and 130 ps. Thus, in order to explain the experimental $\bar{\tau}$ of Fig. 2, a vacancy-type defect must be considered [45].

Regardless of the phase and the parametrization used, the calculated lifetime of V_{Ni} is slightly lower compared to the other ones. Depending on the $\gamma(\mathbf{r})$ parametrization, a clear dispersion is observed. On the one hand, by comparing the shaded area in Fig. 3(c) and the theoretical calculations, it is concluded that $\gamma(\mathbf{r})^{\mathrm{AP1}}_{\mathrm{LDA}}$ and $\gamma(\mathbf{r})^{\mathrm{AP2}}_{\mathrm{LDA}}$ underestimate the positron lifetime. These characteristic lifetimes cannot reproduce the experimental values because of the $\bar{\tau} \leq \tau_v$ constraint [45]. On the other hand, $\gamma(\mathbf{r})^{\mathrm{AP1}}_{\mathrm{GGA}}$ and $\gamma(\mathbf{r})^{\mathrm{AP2}}_{\mathrm{GGA}}$ yield values up to ≈12 ps higher than the experimental ones.

As previously commented, the evolution of the experimental $\bar{\tau}$ is in the saturation trapping regime. In this regime, the contribution of the saturated defect overcomes the bulk contribution and $\bar{\tau}$ reflects the characteristic lifetime that the defect presents, $\bar{\tau} \approx \tau_v$ [45,73]. Along with it, the highest value that has been reached by quenching has always been around 178 ps. Therefore the $\gamma(\mathbf{r})^{\mathrm{BN}}_{\mathrm{LDA}}$ parametrization is the one that predicts best the experimental results [82].

The last column of Table I gathers the calculated positron lifetimes using $\gamma(\mathbf{r})^{\mathrm{BN}}_{\mathrm{LDA}}$. It is worth mentioning that PALS measurements of samples Q1173 and Q873 during IAC were taken at 350 K ($Fm\bar{3}m$ phase). The calculated positron lifetime value of V_{Ni} is the one that best matches sample AQ1173's experimental value, that is 178 ps [see Fig. 3(c)]. Additionally, prior to IAC, both quenched samples were also measured in the $I4/mmm$ phase at 273 K, showing a value of 176 ps for AQ1173 and 174 ps for AQ873 (see Fig. 2, inset, blue shadowed area). As shown in Fig. 3(d), the 176 ps value matches with the calculated value of V_{Ni} in the $I4/mmm$ phase. As a result, the vacancy concentration for AQ1173 is higher than for the one for AQ873 in both phases, as AQ873 shows values below 178 ps in the $Fm\bar{3}m$ and 176 ps in the $I4/mmm$. These results are in good agreement with most predictions of vacancy formation energies in Ni-based Heusler alloys [36–38,40,42], which indicate that Ni is the vacancy that presents the lowest formation energy, ranging between 0.4 and 0.7 eV. Therefore, it can be concluded that V_{Ni} is the most probable vacancy type defect assisting the observed shift in T_{MT}. However, the recently proposed parametrizations for $\gamma(\mathbf{r})$ [83,84] may shed further proof of the vacancy-type defect present in $Ni_{55}Fe_{17}Ga_{28}$.

Finally, taking into account the good agreement between experimental PALS results and DFT calculations, C_v values for samples Q873 and Q1173 can be calculated by means of Eq. (1) using $\tau_b = 106$ and $\tau_v = 178$ ps; see Fig. 2(b). Furthermore, Fig. 4 evidences the mutual dependence of the evolution of T_{MT} and C_v. It is important to notice that the variation of T_{MT} (the recovery of the $L2_1$ order degree assisted by vacancies) is relative to the retained $L2_1$ order degree of the AQ samples. The underlying mechanism by which vacancies drive the ΔT_{MT} may be related to the interaction of vacancies with partial dislocations [35] or vacancies acting as pinning centers [30,85], among others. In particular, Ren and Otsuka [25,26] demonstrate that for the short-range order adaptation between phases, the aging of the sample is needed, which opens a time lag for vacancies to accommodate. The diffusion of point defects to match the new symmetry may be a plausible mechanism by which the MT characteristics are altered. Anyway, as shown by Fig. 4, the present results clearly prove that vacancies play a fundamental role on ΔT_{MT}.

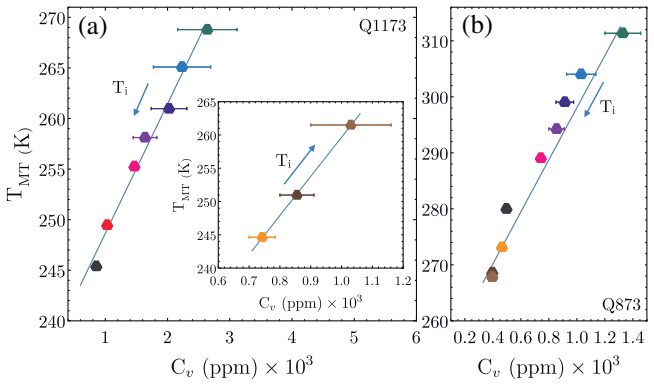

FIG. 4. (a) T_{MT} vs C_v for the Q1173 sample. For a better display, the ranges in which both T_{MT} and C_v increase are shown in the inset. (b) Dependence of C_v and T_{MT} for the Q873 sample. Both curves manifest the mutual dependence between vacancies and ΔT_{MT}.

In sample Q1173, the ordering process during subsequent IAC is accomplished by a reduction of C_v [Fig. 4(a)], which in turn, matches the T_{MT} decrease [see Figs. 1(c) and 1(d)], enhancing the degree $L2_1$ order with the consequent decrease of T_{MT}. Additionally, as shown in the inset of Fig. 4(a), for T_i values between 550 and 600 K, T_{MT} increases with C_v increase. Indeed, the increase of C_v and the increase of T_{MT} take place at the same T_i temperature and the inset shows their correlated evolution.

Regarding sample AQ873, the same behavior is observed. During IAC, T_{MT} decreases monotonically rather than showing a minimum value as C_v does in Q1173. Even so, the vacancy dynamics of sample Q873 follows the same trend of T_{MT}. Figure 4(b) shows their mutual dependence and again, the shift of T_{MT} is directly related with the evolution of C_v. The different evolution that C_v shows in samples Q1173 and Q873 evidences different vacancy dynamics in samples quenched above or below T_{L2_1-B2}, which results in a different evolution of T_{MT}. The mutual dependence of C_v and T_{MT} in both samples do confirm that vacancies play a fundamental role in the evolution of T_{MT}.

In conclusion, we demonstrate experimentally for the first time that vacancies assist the shift of T_{MT}. DSC measurements enable the tracking of T_{MT}, whereas PALS reveals its dependency on C_v. Thereby, the long-standing question of whether the different T_{MT} evolution for samples quenched above or below T_{L2_1-B2} rely on different vacancy dynamics, is answered. Additionally, electron-positron DFT calculations enable the identification of V_{Ni} as the most probable vacancy in the $Ni_{55}Fe_{17}Ga_{28}$ alloy. In summary, this work shows the potential of vacancies for the fine tuning of T_{MT}, enabling shifts in up to ≈50 K. This work opens the way for defect engineering in tuning T_{MT} and the related multifunctional properties of Ni-Fe-Ga alloys.

This work is supported by the Basque Government Grant No. IT-1005-16 and by the Spanish Ministry of Economy and Competitiveness under the Projects No. MAT2015-65165-C2-R (MINECO/FEDER) and No. MAT2014-56116-C4-1-R (AEI/FEDER). I. U. acknowledges the Basque Government Grant No. PRE-2014-214 and the authors thank J. Feuchtwanger for his technical support.

*iraultza.unzueta@ehu.eus

[1] S. Y. Yu, Z. H. Liu, G. D. Liu, J. L. Chen, Z. X. Cao, G. H. Wu, B. Zhang, and X. X. Zhang, Appl. Phys. Lett. **89**, 162503 (2006).
[2] S. Banik, R. Rawat, P. K. Mukhopadhyay, B. L. Ahuja, A. Chakrabarti, P. L. Paulose, S. Singh, A. K. Singh, D. Pandey, and S. R. Barman, Phys. Rev. B **77**, 224417 (2008).
[3] A. Planes, L. Mañosa, and M. Acet, J. Phys. Condens. Matter **21**, 233201 (2009).
[4] L. Mañosa, D. González-Alonso, A. Planes, E. Bonnot, M. Barrio, J.-L. Tamarit, S. Aksoy, and M. Acet, Nat. Mater. **9**, 478 (2010).
[5] K. Ullakko, J. K. Huang, C. Kantner, R. C. O'Handley, and V. V. Kokorin, Appl. Phys. Lett. **69**, 1966 (1996).
[6] M. Chmielus, X. X. Zhang, C. Witherspoon, D. C. Dunand, and P. Müllner, Nat. Mater. **8**, 863 (2009).
[7] Y. Sutou, Y. Imano, N. Koeda, T. Omori, R. Kainuma, K. Ishida, and K. Oikawa, Appl. Phys. Lett. **85**, 4358 (2004).
[8] M. Ye, A. Kimura, Y. Miura, M. Shirai, Y. T. Cui, K. Shimada, H. Namatame, M. Taniguchi, S. Ueda, K. Kobayashi, R. Kainuma, T. Shishido, K. Fukushima, and T. Kanomata, Phys. Rev. Lett. **104**, 176401 (2010).
[9] E. Şaşıoğlu, L. M. Sandratskii, and P. Bruno, Phys. Rev. B **77**, 064417 (2008).
[10] S. Fujii, S. Ishida, and S. Asano, J. Phys. Soc. Jpn. **58**, 3657 (1989).
[11] C. Tan, Z. Tai, K. Zhang, X. Tian, and W. Cai, Sci. Rep. **7**, 43387 (2017).
[12] P. Álvarez-Alonso, C. Aguilar-Ortiz, E. Villa, A. Nespoli, H. Flores-Zúñiga, and V. Chernenko, Scr. Mater. **128**, 36 (2017).
[13] Y. Xu, B. Lu, W. Sun, A. Yan, and J. Liu, Appl. Phys. Lett. **106**, 201903 (2015).
[14] S. Chabungbam, P. Borgohain, S. Ghosh, N. Singh, and M. B. Sahariah, J. Alloys Compd. **689**, 199 (2016).
[15] J. Pons, E. Cesari, C. Seguí, F. Masdeu, and R. Santamarta, Mater. Sci. Eng. A **481–482**, 57 (2008).
[16] Y. Li, D. Zhao, and J. Liu, Sci. Rep. **6**, 25500 (2016).
[17] S. Chabungbam, S. Gowtham, and M. B. Sahariah, Phys. Rev. B **89**, 085114 (2014).
[18] K. Oikawa, Y. Imano, V. A. Chernenko, F. Luo, T. Omori, Y. Sutou, R. Kainuma, T. Kanomata, and K. Ishida, Mater. Trans., JIM **46**, 734 (2005).
[19] H. Morito, A. Fujita, K. Oikawa, K. Fukamichi, R. Kainuma, T. Kanomata, and K. Ishida, J. Phys. Condens. Matter **21**, 076001 (2009).
[20] K. Oikawa, T. Ota, T. Ohmori, Y. Tanaka, H. Morito, A. Fujita, R. Kainuma, K. Fukamichi, and K. Ishida, Appl. Phys. Lett. **81**, 5201 (2002).

[21] H. R. Zhang, C. Ma, H. F. Tian, G. H. Wu, and J. Q. Li, Phys. Rev. B **77**, 214106 (2008).
[22] Z. H. Liu, H. N. Hu, G. D. Liu, Y. T. Cui, M. Zhang, J. L. Chen, G. H. Wu, and G. Xiao, Phys. Rev. B **69**, 134415 (2004).
[23] Y. Qawasmeh and B. Hamad, J. Appl. Phys. **111**, 033905 (2012).
[24] V. Recarte, J. Pérez-Landazábal, V. Sánchez-Alarcos, and J. Rodríguez-Velamazán, Acta Mater. **60**, 1937 (2012).
[25] X. Ren and K. Otsuka, Nature (London) **389**, 579 (1997).
[26] X. Ren and K. Otsuka, Phys. Rev. Lett. **85**, 1016 (2000).
[27] Y. Zhang, L. Zhang, Q. Zheng, X. Zheng, M. Li, J. Du, and A. Yan, Sci. Rep. **5**, 11010 (2015).
[28] Z. ni Zhou, L. Yang, J. ge Wang, T. Jin, Y. Huang, J. Li, Q. Hu, and J. guo Li, Prog. Nat. Sci. Mater. **27**, 356 (2017).
[29] S. Kustov, J. Pons, E. Cesari, and J. V. Humbeeck, Acta Mater. **52**, 3075 (2004).
[30] S. Kustov, J. Pons, E. Cesari, and J. V. Humbeeck, Acta Mater. **52**, 3083 (2004).
[31] V. Sánchez-Alarcos, V. Recarte, J. Pérez-Landazábal, and G. Cuello, Acta Mater. **55**, 3883 (2007).
[32] J. Font, J. Muntasell, R. Santamarta, J. Pons, E. Cesari, V. Recarte, J. Pérez-Landazábal, C. Gómez-Polo, and J. Dutkiewicz, Mater. Sci. Eng. A **481–482**, 262 (2008).
[33] R. Santamarta, E. Cesari, J. Font, J. Muntasell, J. Pons, and J. Dutkiewicz, Scr. Mater. **54**, 1985 (2006).
[34] K. Oikawa, T. Omori, Y. Sutou, H. Morito, R. Kainuma, and K. Ishida, Metall. Mater. Trans. A **38**, 767 (2007).
[35] T. Y. Hsu and Y. Linfah, J. Mater. Sci. **18**, 3213 (1983).
[36] J. Bai, J. M. Raulot, Y. D. Zhang, C. Esling, X. Zhao, and L. Zuo, J. Appl. Phys. **108**, 064904 (2010).
[37] J. Bai, N. Xu, J.-M. Raulot, Y. D. Zhang, C. Esling, X. Zhao, and L. Zuo, J. Appl. Phys. **113**, 174901 (2013).
[38] J. Bai, N. Xu, J. M. Raulot, C. Esling, X. Zhao, and L. Zuo, Int. J. Quantum Chem. **113**, 847 (2012).
[39] S. Kulkova, S. Eremeev, S. Kulkov, and V. Skripnyak, Mat. Sci. Eng. A **481–482**, 209 (2008).
[40] S. Kulkova, S. Eremeev, Q. Hu, C. Li, and R. Yang, in *ESOMAT 2009 (Czech Republic, 2009)*, (EDP Sciences, Les Ulis, France, 2009), p. 02017.
[41] A. Kosogor, V. V. Sokolovskiy, V. A. L'vov, and V. V. Khovaylo, Phys. Status Solidi B **252**, 2309 (2015).
[42] Y. Wang, D. Salas, B. Medasani, P. Entel, I. Karaman, R. Arróyave, and T. C. Duong, Phys. Status Solidi B **255**, 1700523 (2018).
[43] D. Merida, J. García, V. Sánchez-Alarcos, J. Pérez-Landazábal, V. Recarte, and F. Plazaola, J. Alloys Compd. **639**, 180 (2015).
[44] D. Merida, J. A. García, V. Sánchez-Alarcos, J. I. Pérez-Landazábal, V. Recarte, and F. Plazaola, Appl. Phys. Lett. **104**, 231905 (2014).
[45] See Supplemental Material at http://link.aps.org/supplemental/10.1103/PhysRevLett.122.165701 for details of the synthesis and PALS experiments, for the exact expressions used in the modeling of $\gamma(\mathbf{r})$, and for the determination of vacancy concentration from the experimentally measured average positron lifetime, which includes Refs. [46–64].
[46] J. M. Barandiarán, V. A. Chernenko, P. Lázpita, J. Gutiérrez, and J. Feuchtwanger, Phys. Rev. B **80**, 104404 (2009).
[47] P. Kirkegaard and M. Eldrup, Comput. Phys. Commun. **7**, 401 (1974).
[48] M. Bertolaccini and L. Zappa, Nuovo Cimento B **52**, 487 (1967).
[49] B. Somieski, T. Staab, and R. Krause-Rehberg, Nucl. Instrum. Methods Phys. Res., Sect. A **381**, 128 (1996).
[50] K. Plotkowski, T. Panek, and J. Kansy, Nuovo Cimento D **10**, 933 (1988).
[51] I. MacKenzie and J. Fabian, Nuovo Cimento B **58**, 162 (1980).
[52] R. M. Nieminen, E. Boronski, and L. J. Lantto, Phys. Rev. B **32**, 1377 (1985).
[53] E. Boroński and R. M. Nieminen, Phys. Rev. B **34**, 3820 (1986).
[54] J. Arponen and E. Pajanne, Ann. Phys. (N.Y.) **121**, 343 (1979).
[55] L. J. Lantto, Phys. Rev. B **36**, 5160 (1987).
[56] B. Barbiellini, M. J. Puska, T. Torsti, and R. M. Nieminen, Phys. Rev. B **51**, 7341 (1995).
[57] J. M. C. Robles, E. Ogando, and F. Plazaola, J. Phys. Condens. Matter **19**, 176222 (2007).
[58] G. E. Kimball and G. H. Shortley, Phys. Rev. **45**, 815 (1934).
[59] W. Brandt and R. Paulin, Phys. Rev. B **5**, 2430 (1972).
[60] M. Puska and R. Nieminen, Rev. Mod. Phys. **66**, 841 (1994).
[61] K. Saarinen, P. Hautojärvi, A. Vehanen, R. Krause, and G. Dlubek, Phys. Rev. B **39**, 5287 (1989).
[62] C. Corbel, F. Pierre, K. Saarinen, P. Hautojärvi, and P. Moser, Phys. Rev. B **45**, 3386 (1992).
[63] F. Plazaola, K. Saarinen, L. Dobrzynski, H. Reniewicz, F. Firszt, J. Szatkowski, H. Meczynska, S. Legowski, and S. Chabik, J. Appl. Phys. **88**, 1325 (2000).
[64] R. Krause-Rehberg, A. Polity, W. Siegel, and G. Kuhnel, Semicond. Sci. Technol. **8**, 290 (1993).
[65] V. Sánchez-Alarcos, J. I. Pérez-Landazábal, V. Recarte, J. A. Rodríguez-Velamazán, and V. A. Chernenko, J. Phys. Condens. Matter **22**, 166001 (2010).
[66] V. Sánchez-Alarcos, V. Recarte, J. Pérez-Landazábal, C. Gómez-Polo, and J. Rodríguez-Velamazán, Acta Mater. **60**, 459 (2012).
[67] V. Sánchez-Alarcos, J. Pérez-Landazábal, V. Recarte, I. Lucia, J. Vélez, and J. Rodríguez-Velamazán, Acta Mater. **61**, 4676 (2013).
[68] V. Sánchez-Alarcos, J. Pérez-Landazábal, C. Gómez-Polo, and V. Recarte, J. Magn. Magn. Mater. **320**, e160 (2008).
[69] C. Picornell, J. Pons, E. Cesari, and J. Dutkiewicz, Intermetallics **16**, 751 (2008).
[70] R. Santamarta, J. Font, J. Muntasell, F. Masdeu, J. Pons, E. Cesari, and J. Dutkiewicz, Scr. Mater. **54**, 1105 (2006).
[71] P. Hautöjarvi, *Positrons in Solids*, Topics in Current Physics (Springer, Heidelberg, 1979), Vol. 12.
[72] B. Barbiellini, in *New Directions in Antimatter Chemistry and Physics*, edited by C. M. Surko and F. A. Gianturco (Kluwer Academic Publishers, Dordrecht, 2001), p. 127.
[73] F. Tuomisto and I. Makkonen, Rev. Mod. Phys. **85**, 1583 (2013).
[74] T. E. M. Staab, R. Krause-Rehberg, B. Vetter, and B. Kieback, J. Phys. Condens. Matter **11**, 1807 (1999).
[75] H.-E. Schaefer, Phys. Status Solidi A **102**, 47 (1987).

[76] P. J. Brown, A. P. Gandy, K. Ishida, R. Kainuma, T. Kanomata, H. Morito, K.-U. Neumann, K. Oikawa, and K. R. A. Ziebeck, J. Phys. Condens. Matter **19**, 016201 (2007).
[77] M. J. Puska and R. M. Nieminen, J. Phys. F **13**, 333 (1983).
[78] B. Barbiellini, M. J. Puska, T. Korhonen, A. Harju, T. Torsti, and R. M. Nieminen, Phys. Rev. B **53**, 16201 (1996).
[79] T. Korhonen, M. J. Puska, and R. M. Nieminen, Phys. Rev. B **54**, 15016 (1996).
[80] I. Unzueta, N. Zabala, V. Marín-Borrás, V. Muñoz-Sanjosé, J. A. García, and F. Plazaola, Phys. Rev. B **94**, 014117 (2016).
[81] J. Bai, Y. Chen, Z. Li, P. Jiang, P. Wei, and X. Zhao, AIP Adv. **6**, 125007 (2016).
[82] I. Unzueta, V. Sánchez-Alarcos, V. Recarte, J. I. Pérez-Landazábal, N. Zabala, J. A. García, and F. Plazaola, Phys. Rev. B **99**, 064108 (2019).
[83] B. Barbiellini and J. Kuriplach, Phys. Rev. Lett. **114**, 147401 (2015).
[84] N. D. Drummond, P. López Ríos, R. J. Needs, and C. J. Pickard, Phys. Rev. Lett. **107**, 207402 (2011).
[85] A. Mansouri Tehrani, H. Shahrokhshahi, N. Parvin, and J. Brgoch, J. Appl. Phys. **118**, 014901 (2015).